ADVANCED MATERIALS
www.advmat.de

High-Density Soft-Matter Electronics with Micron-Scale Line Width

B. Arda Gozen, Arya Tabatabai, O. Burak Ozdoganlar, and Carmel Majidi**

This paper presents a new method for fabricating soft and stretchable liquid-phase microelectronics that feature circuit elements with micron-scale line width. In contrast to conventional microelectronics, these circuits are composed of a soft elastomer embedded with microfluidic channels filled with eutectic Gallium-Indium (EGaIn) metal alloy. The EGaIn traces are liquid at room temperature and therefore remain intact and electrically functional as the surrounding elastomer elastically deforms during stretching and bending. The fabrication method uses emerging techniques in soft lithography. Microchannels are molded on to the surface of poly(dimethylsiloxane) (PDMS) elastomer and filled with EGaIn using a micro-transfer deposition step that exploits the unique wetting properties of EGaIn in air. After sealing with an addition layer of PDMS, the liquid-filled channels function as stretchable circuit wires or capacitor electrodes. The presented approach allows for the creation of micron-scale circuit features with a line width (2 μm) and spacing (1 μm) that is an order-of-magnitude smaller than those previously demonstrated.

Eutectic Gallium-Indium (EGaIn)-based electronics are composed of microchannels filled with EGaIn that are sealed in a soft elastomer. These soft and stretchable circuits remain mechanically intact and electrically functional under extreme elastic deformation.[1–3] This intrinsic elasticity enables compliance matching with human tissue[4–6] and allows EGaIn electronics to complement metal-coated textiles, wavy circuits, and other elastically-deformable technologies that can be worn on the skin or implanted in the body without interfering with natural bodily functions. Previous applications include antennae for wireless communication,[7,8] diodes and memristors for circuit logic,[9,10] and strain, force and pressure sensors for measuring human joint motion and detecting skin contact.[11–14]

As a non-toxic alternative to mercury, Gallium-Indium alloys such as EGaIn, Gallium-Indium-Tin (Galinstan®), NewMerc, and Indalloy are particularly attractive for their high electrical conductivity ($\sigma = 3.4 \times 10^6$ S/m), which is $1/20^{th}$ the conductivity of copper and is orders of magnitude greater than conductive grease and electrolytic solutions.[15,16] In addition to being liquid at room temperature (MP < 15 °C), GaIn alloys form an oxide layer in air that enables higher wettability on non-metallic surfaces[17] and allows them to retain their shape and form stable free-standing structures.[1,15–19] This property as a "moldable liquid" has enabled a broad range of planar and 3D patterning methods, including mask stencil lithography,[13,20,21] droplet-based transfer microcontact printing (μCP),[22] freeze-casting,[23] laser engraving,[24] and deposition with 3D printing.[25,26] Aforementioned patterning techniques have only been used to produce circuits with feature sizes greater than 30 μm. The main limitation for those techniques is that they generally involve injection of liquid alloys under pressure into micro-channels or onto target elastomeric surfaces. In both cases, creation of single-micron scale structures requires very high pressures that can exceed the elastic modulus of the elastomer and lead to mechanical failure. Dickey et al.[18] reported that the pressure required to inject EGaIn into microchannels can be calculated using the Young's-Laplace equation. Using this equation, the pressure required to inject EGaIn into the channels with width of a few microns is calculated as greater than 1 MPa, which is above the failure limit of elastomers. Accordingly, there is a need for new methods for the fabrication of soft and stretchable *microelectronics* with single micron-scale line widths to enable the high circuit-density and sophisticated functionality of conventional rigid microelectronics.

In this paper, we present the fabrication and initial testing of EGaIn-based high-density stretchable microelectronic components with line width and spacing as small as 2 μm and 1 μm, respectively. The fabrication method is illustrated in **Figure 1**(a). In this approach, the first step is to create an elastomer mold with micron-scale concave features (i.e., micro-channels) through elastomer replica molding.[27,28] Next, the liquid-phase EGaIn (Gallium-Indium eutectic; ≥99.99%; Sigma-Aldrich) is spread across an elastomeric "donor" substrate using a roller. The deposited EGaIn is then flattened by compression using a flat elastomeric substrate under normal force. Next, the elastomer mold is pressed onto the EGaIn film, allowing the liquid alloy to fill the microchannels. This process is similar to imprint lithography processes,[29] where the EGaIn film flows to conform to the geometry of the elastomer mold surface under the applied pressure. When the elastomer mold is separated from the donor substrate, the channels remain filled with EGaIn. We attribute this selective wetting of the micro-channels to the existence of the oxide skin that forms on the inside surface of the channels (i.e. channel walls). We base this hypothesis on a previous study by Dickey et al.[18] which concluded that when injected into microchannels, the oxide skin causes the EGaIn to remain inside even when the injection pressure is removed. Lastly, the EGaIn-filled microchannels are sealed with an additional layer of elastomer. This versatile fabrication technique could be used to pattern EGaIn into any planar network of microfluidic channels that is cast into an elastomer mold.

Dr. B. A. Gozen, A. Tabatabai,
Prof. O. B. Ozdoganlar, Prof. C. Majidi
Carnegie Mellon University
Mechanical Engineering Department
5000 Forbes Avenue, Scaife Hall
Pittsburgh, PA 15213, USA
E-mail: burakoz@andrew.cmu.edu;
cmajidi@andrew.cmu.edu

DOI: 10.1002/adma.201400502

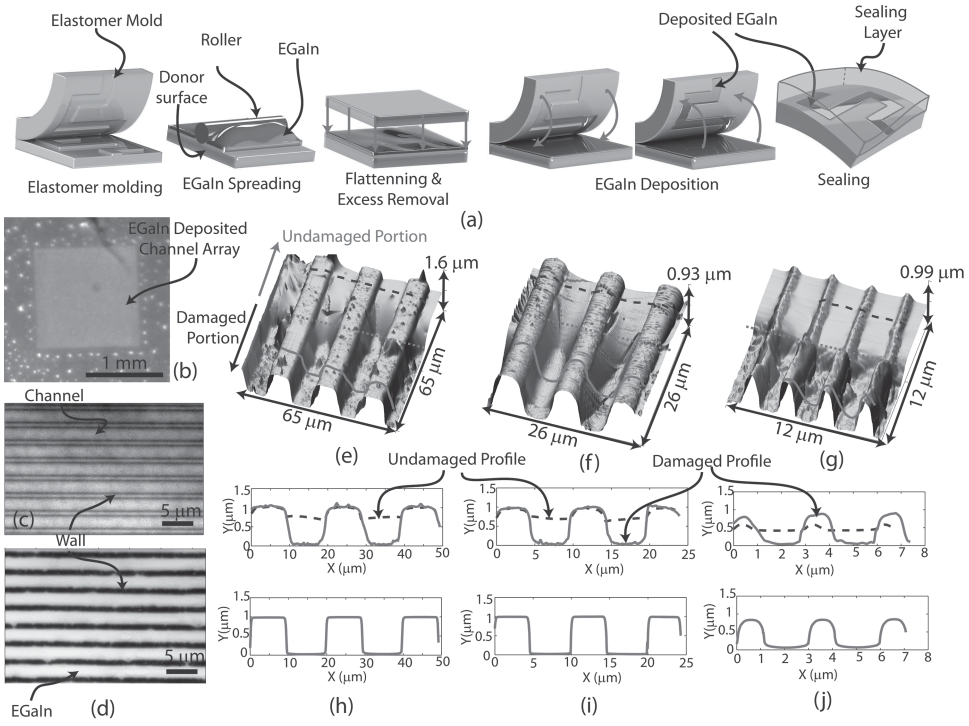

Figure 1. (a) Schematic description of the EGaIn deposition process; (b) a stereo microscope image of the area with EGaIn deposited channel array and light intensity maps of the optical interferometry measurements of the elastomeric substrate with periodic 2 µm wide trenches; (c) prior to EGaIn deposition; (d) after EGaIn deposition; (e-g) three-dimensional AFM images of the partially emptied channels having widths of 10 µm, 5 µm, 2 µm, respectively; (h-j) cross-sectional AFM data from the undamaged and damaged sections of the channels (top), cross-sectional AFM profile of the channels prior to EGaIn deposition (bottom), corresponding to channels having widths of 10 µm, 5 µm, 2 µm, respectively.

To demonstrate this method, we used a PDMS mold patterned with arrays of channels having a nominal depth of 1 µm and length of 1.5 mm. Three different channel-width and inter-channel spacing combinations were included on the mold: 10 µm width with 10 µm spacing; 5 µm width with 5 µm spacing; and 2 µm width with 1 µm spacing. A PDMS donor substrate was used during the process. As shown in Figure 1(b), the micro-patterned EGaIn can be clearly seen over a large (approximately 4 mm^2) surface area. The light intensity maps acquired from optical profilometry (Zygo NewView 7300) of the 2 µm wide channels before and after EGaIn deposition is given by Figures 1(c) and 1(d), respectively. In these figures, EGaIn filled channels are recognized by higher light intensity (white color). Higher resolution description of the channels deposited with EGaIn is provided by their SEM images in Figure S1 of the supporting information. The presented method can also be used to deposit EGaIn into square-shaped holes and "around" square-shaped pillars (i.e., protrusions) as shown in Figure S2(a) and (b) in the supporting information, respectively. We also made few attempts to deposit EGaIn into arrays of channels that are 1 µm wide and with an inter-channel spacing of 2 µm. The obtained results are presented in Figure S2(c)-(e) in the supporting information. In this case, we did not observe continuous wires across wire lengths of more than a few tens of microns. Furthermore, the line-widths were not consistent throughout the sample.

To better understand the filling characteristics of the microchannels, we locally and selectively removed a portion of the deposited EGaIn patterns prior to sealing using a sharp tungsten probe with a sub-micron tip radius. The regions that include the interface between the removed (damaged) and undamaged EGaIn patterns (Figures 1(e)–1(g)) were analyzed using atomic force microscopy (AFM). Cross-sectional profiles of the channels prior to EGaIn deposition are also provided in Figures 1(h)–1(j). As shown, the EGaIn fills the channels, forming "wires" of EGaIn along the length of the channels. However, the depths of the EGaIn lines (i.e., the thickness of the wires) are shallower than the depth of the channels. One possible reason for this height difference may be the elastic deformation of the channel walls during the contact deposition. The height difference was seen to depend on the channel width, and may also be a function of the rate at which the normal force is released and the mold is separated from the EGaIn film. Furthermore, outside the channels (on the tops of the walls that separate the channels), a thin residual layer of EGaIn is observed. It is seen that this residual layer causes deformation of the sidewalls, particularly for the channel arrays with 1 µm spacing (Figure 1(j)). For channel arrays with larger spacing, periodic textures are observed on the tops of the channel spacing walls (see Figure S3(a) in the supporting information). AFM measurements indicated that the thickness of the residual layer is approximately 10 nm (see Figure S3(b) in the supporting information). The residual layer is optically transparent, although not as transparent as clean PDMS, as shown in Figure S3(c). High-resolution SEM images presented in Figure S1 of the supporting information show the

Adv. Mater. **2014**,
DOI: 10.1002/adma.201400502

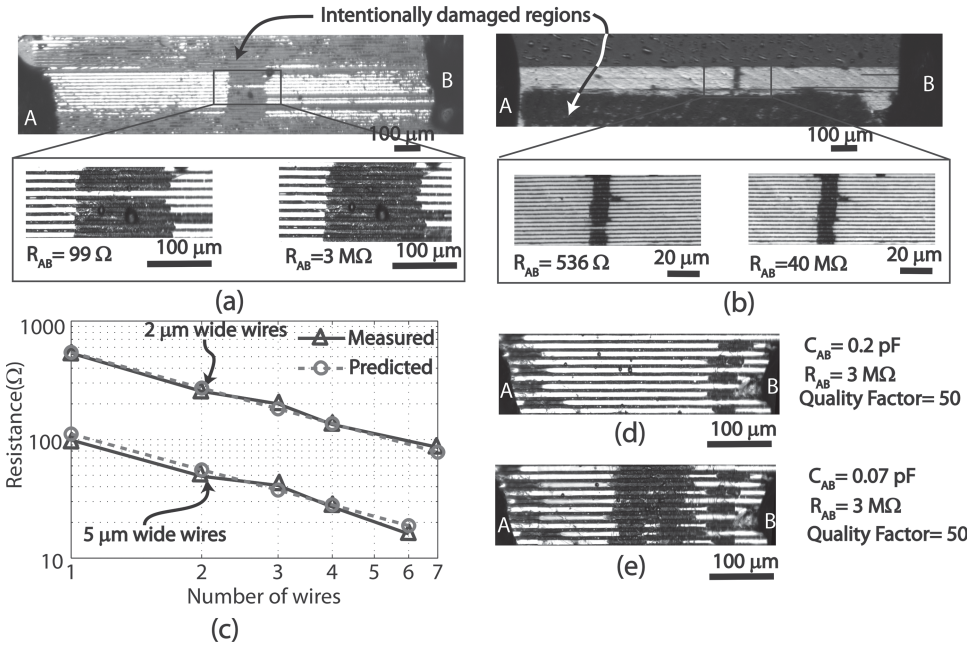

Figure 2. Microscope images of the EGaIn wire arrays with linewidths of (a) 5 µm, (b) 2 µm that are tested during resistance measurements; (c) measured values (solid) and Ohm's Law-based predictions (dashed) for the resistances of 5 µm and 2 µm wide wires for different number of wires connected in parallel; and (d) microscope images of the interdigital co-planar capacitor created through local disconnection of the 5 µm wide wires and associated capacitance measurements.

sub-micron sized EGaIn droplets that are also observed on the residual layer.

To study the electrical characteristics of the patterned EGaIn, we performed conductivity measurements on 5 µm and 2 µm wide wires. As shown in **Figures 2**(a) and 2(b), we isolated a limited number of wires by intentionally damaging their neighboring wires. Detailed microscopy images of the tested 2 µm wide wire array, taken at different magnifications, are presented in Figure S4 of the supporting information. To perform the measurements, tungsten probes were inserted into two large droplets of EGaIn, administered at the end of the isolated wires prior to sealing. During the measurements, the inherent resistance of the measurement loop (resistance of the probes, contact resistance between the probes and the droplets etc.) were quantified and subtracted from the measured resistance. To correlate the resistance values with the number of EGaIn wires, we used a sequential approach: The resistance was first measured for the largest number of wires. For each of the following measurements, one wire was severed using the tungsten probe before each measurement. Approximately six orders of magnitude increase in the measured resistance was observed after the disconnecting all the wires for both of the studied cases.

To compare the conductivity of the created EGaIn microwires with the bulk conductivity of EGaIn, we compared the measured resistance values with values that were predicted using Ohm's Law. The predicted resistance values were calculated as

$$R = \left(\sum_{i=1}^{n} \frac{1}{R_i} \right)^{-1}, \quad (1)$$

where n is the number of the wires connected in parallel and R_i is the individual resistance of the measured wires,

$$R_i = \rho \int_0^L \frac{dx}{A_i(x)} \quad (2)$$

Here, ρ is the volume resistivity of EGaIn (29.4×10^{-6} Ω.cm[30],) x is the coordinate along the length of a wires, L is the total length of the wire, and $A_i(x)$ is the cross-sectional area of the wire at a coordinate x along the length of the wire. To determine $A_i(x)$, optical profilometry measurements of the wires were conducted both before and after the wires were disconnected (i.e., destroyed with the tungsten probe). Assuming that the channels were filled entirely below the measured top surface, the cross-sectional area at a given location was calculated by integrating the difference between the filled and emptied cross-sections of the channels. As shown in Figure 2(c), the measured and predicted resistance values show a strong agreement for both wire sizes.

A number of critical conclusions can be drawn from the results of the conductivity test and the agreement between the measured values of wire resistances and the predictions based on Ohm's Law: (1) the micro-wires exhibit the same level of electrical conductivity as bulk EGaIn; (2) the channels on the elastomer mold are completely filled below the surface of the deposited EGaIn; (3) the wires are not shorting across the inter-wire spacing, which can be as small as 1 µm with our method. The last conclusion follows from the strong agreement between the predicted and measured resistances for multiple parallel wires and the dramatic increase in resistance after the wires are disconnected. From this observation, we also postulate that the residual layer between the

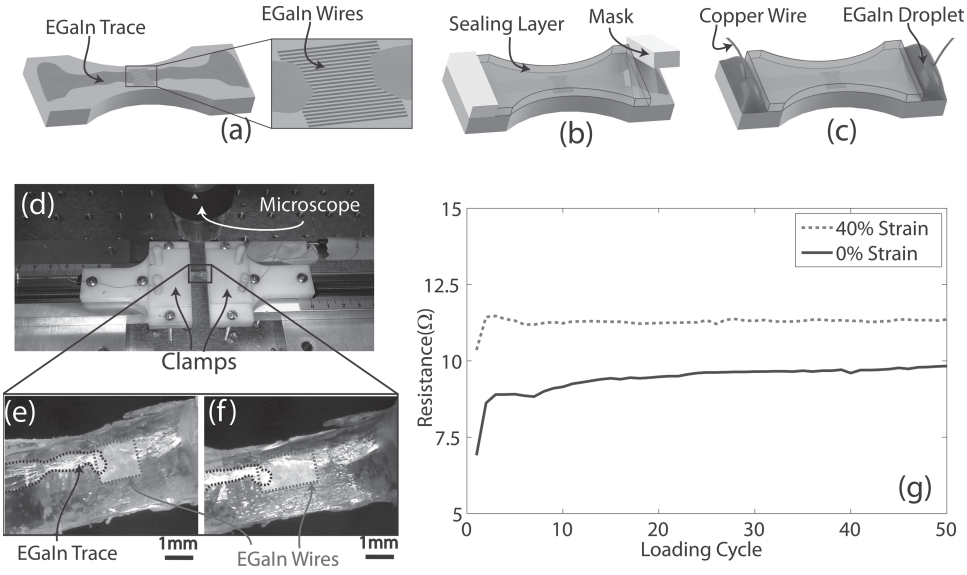

Figure 3. (a) Schematic of the test sample prior to sealing and after the application of EGaIn traces; (b) Sealing using masks at the end of the EGaIn traces; (c) application of the EGaIn droplets on the exposed traces and insertion of copper wires; (d) Axial testing setup; Stereo microscopy images of the test sample at (e) 0% strain, (f) 40% strain; (g) The resistance values measured across the test sample at different deformation cycles.

channels mostly consists of non-conductive oxides of gallium (Ga_2O_3).

An example of a functional circuit element that can be created using the presented technique is a co-planar capacitor.[31] To demonstrate this application, a co-planar capacitive structure shown in Figure 2(d) was created. For this purpose, 5 μm wide wires with 5 μm spacing were selectively disconnected (i.e., damaged with tungsten probes) to form a comb pattern with a total of ten fingers. The results of the capacitance measurements across the EGaIn droplets at both ends of the structure and the associated quality factors are also provided in Figure 2(d). To quantify any parasitic capacitive effect (e.g., those due to the applied droplets or the residual layer), we performed another capacitance measurement after disconnecting all the fingers, as given in Figure 2(e). Assuming a parallel electrical connection between the co-planar capacitance of the created structure and the parasitic capacitance, we concluded that the effective capacitance of the EGaIn-based capacitor is 0.13 pF. We then compared this value to a co-planar capacitance model by Gevorgian et al.,[31] which predicted the capacitance as 0.08 pF. The coplanar interdigitated capacitor models in the literature make a number of assumptions that may lead to lower reliability, especially for low capacitance. Other sources of uncertainty include the dielectric constant of the elastomer and the neglected dielectric effect of the residual layer. Considering such uncertainties, the measured capacitance value can be considered as reasonable. The total surface area within which the measured capacitance is achieved is approximately 2×10^{-8} m^2, yielding a density of capacitance over the planar area as high as 6.5 μF/m^2. This is significantly higher than the ~10 nF/m^2 capacitance density previously achieved with EGaIn-based soft-matter electronics.[32] This result clearly indicates that, through proper design of the micro-channel network on the elastomer mold, the presented fabrication method can be used to create micron-scale strain gages, pressure sensors, RLC circuits and antennae for remote sensing and wireless communication. Such a capability will enable high-density microelectronics implementations for flexible and stretchable devices.

One of the key requirements for soft-matter electronics is for them to maintain their electronic functionality during elastic deformation. To study the behavior of the fabricated EGaIn wires under mechanical strains, we performed an axial loading test on the EGaIn deposited substrates (5 μm wide wires were tested). To enable conductivity measurements during the mechanical testing, flat traces of EGaIn are administered at both ends of the wires prior to sealing (**Figure 3**(a)). These traces were extended to both ends of the test sample, and were masked before the application of the uncured PDMS sealing layer. After the sealing layer is cured, the masks were removed to expose the ends of the EGaIn traces (Figure 3(b)). Larger EGaIn droplets were then administered on the exposed trace, creating two electrodes that allow copper wires to be inserted in to perform resistance measurements (Figure 3(c)). The sealed elastomeric substrate was clamped at its two ends in a horizontal configuration as shown in Figure 3(d). In this configuration, the left clamp was kept stationary, whereas the right clamp was moved horizontally, thereby stretching the substrate. The samples were stretched to a maximum strain of 40% and cyclic axial loading is applied to a total of 50 cycles. The magnified stereo microscopy images of the tested sample at 0 and 40% strain are given by Figure 3(e) and 3(f), respectively.

As shown in Figure 3(g), the resistance values measured across the sample at 0% and 40% strain levels varied noticeably within the first few cycles of elastic deformation and then remained approximately constant for the rest of the testing. The reduction of the sample's conductivity within the first few deformation cycles, may be attributed to the initial deformation/failure of the oxide skin. Specifically, additional exposure of the EGaIn to oxygen during strain may increase the relative amount of Ga_2O_3 within the wire. After the steady-state is

Adv. Mater. **2014**,
DOI: 10.1002/adma.201400502

reached, the resistance values for the 0% and 40% were 9.54 Ω and 11.27 Ω, respectively. This result clearly indicates that the EGaIn wires fabricated using the presented method, maintain their electrical functionality after multiple cycles of elastic deformation. Furthermore, the successful measurement of the electrical resistance of the EGaIn micro-wires interfaced with the air-dispensed EGaIn traces demonstrates a feasible method of using 3D printed interconnects between the micro-wires and any other electrical component.

In summary, we demonstrate the fabrication of elastomer embedded electrically conductive EGaIn structures with sub-micron level depths, line-widths as small as 2 μm, and inter-line spacing as small as 1 μm. This was accomplished by a novel micro-transfer deposition method, where the EGaIn is deposited in micro-patterned features on the surface of an elastomeric substrate. We showed that the EGaIn wires with a length of over 1 mm exhibit the same level of electrical conductivity as that of bulk EGaIn. Accordingly, the fabricated wires can be utilized to create micro-electronic circuit elements, leading to substantial increase in the surface density of the liquid-metal alloy based soft-matter electronics. As an example, we demonstrated fabrication of a co-planar capacitor, which exhibited a 650× increase in capacitance density compared to EGaIn-based circuits previously produced with needle injection. Finally, we showed that the fabricated EGaIn wires can maintain their electrical functionality after 50 cycles of elastic axial deformation with strains up to 40%. This suggests a great potential for realizing high-density microelectronics that are highly flexible, stretchable, elastic, and soft. Nonetheless, in its current form, our fabrication method does not involve a precise control of a number of process parameters. This includes the EGaIn film thickness and uniformity, magnitude and the distribution of the force applied during the contact between the elastomer mold and the EGaIn film, chemistry of the donor and elastomer mold surface, and environmental conditions (e.g. oxygen content). Future work will involve studies that examine the effect of such process parameters on the quality of deposition. Next, the fabrication system will be improved such that it can precisely monitor and control deposition pressure and reliably execute different steps of the fabrication process (e.g., rolling, flattening of the EGaIn film, and micro transfer deposition). We believe that such improvements will help improve repeatability, reduce the number of defects observed over larger surface areas, and improve the resolution of the process down to sub-micron linewidths. This effort will enable scalable fabrication of intelligent soft-matter electronic devices that exhibit a broad range of circuit, sensing, and electromechanical functionalities.

Experimental Section

EGaIn Deposition Process: The elastomer mold was fabricated by a two-step replica molding process. In the first step, an AFM height standard containing thermally grown silicon dioxide features on a silicon substrate (AppNano SHS-1) was molded by a UV-curable polymer (Norland Adhesives NOA-63) to create its negative replica. For this purpose, the liquid precursor was applied on the silicon sample and cured using a UV light source (Black Ray UV-light, 365 nm wavelength) at 21.750 mW-cm^{-2}. The created production mold was then molded by two part PDMS (Slygard 184 Dow Corning, 10:1 mass ratio) to produce the elastomer mold. The PDMS donor substrate was created by curing two-part PDMS against a flat silicon wafer using a larger mass ratio (15:1), which was observed to improve wettability by EGaIn compared to 10:1 mass ratio. A droplet of EGaIn (Ga-In Eutectic, >%99.99, Sigma Aldrich) was introduced on the donor substrate using a syringe and manipulated by a roller to form a smooth (40 nm Ra characterized by optical profilometry) thin film. Both the roller and the flat elastomer substrate used to spread and flatten the EGaIn film were made of PDMS (10:1 mass ratio). The elastomer mold was glued to a glass slide and then attached to a motorized vertical stage (ThorLabs MTS/50-Z8) that was used to establish controllable contact between the mold and the EGaIn film. The donor substrate was attached to a kinematic mount (ThorLabs K6XS), which enabled making angular alignments between the mold and donor substrate. The EGaIn deposited molds were then sealed through polymerization of the sealing PDMS layer (10:1 mass ratio) on the mold. All PDMS samples were polymerized at 50 °C for 8 hours.

Topographical and Optical Characterization of the Deposited EGaIn: The deposited EGaIn was disturbed locally using an ultra-sharp, high-compliance tungsten probe (PicoProbe model T-4-10) having sub-micron tip radii, attached to a three-axis positioning stage. The AFM measurements were conducted in the non-contact mode using high aspect ratio conical probes (Aspire CT300). A specialized AFM system (Park Systems XE-70) that is equipped with an interferometric sensor measuring Z-scanner head motions was used during the measurements. Monitoring of this external sensor's measurement instead of the conventional topography signal enabled accurate height measurements above 1 μm without dealing with the non-linearity of the piezo-scanner. Optical profilometry of the substrates were performed using a white light interferometry system (Zygo NewView 7300) with an optical magnification of 100X or higher. Optical microscopy images were acquired using infinity corrected, long working distance objectives (Mitutoyo M Plan APO NIR) with varying magnifications of 5X, 20X and 50X. Scanning electron microscopy (SEM) imaging of the samples was performed using an FEI Quanta 600 environmental SEM at a low vacuum mode with 0.75 Torr chamber pressure.

Electrical Characterization: The terminal droplets were administered to the ends of the tested EGaIn wires using an air powered dispenser system (Nordson EFD Ultimus 5), which uses a nozzle with 100 μm inner diameter. The administered droplets were spherical in shape, with an approximate diameter of 150 μm. Two tungsten probes with sub-micron tip radii (Micromanipulator Model 7C) attached to two three-axis positioning stages were used for electrical measurements. Both probes were connected to an LCR meter (LBK Precision 889B). To quantify the resistance of the measurement loop primarily consisting of the contact resistance between the EGaIn droplets and the probe tips, two probes were inserted into the same droplet prior to every measurement. The measured resistance varied between 5–10 Ω. The capacitance measurements were conducted in the parallel mode by exciting the capacitor at 1 V amplitude and 2 kHz frequency. Prior to the capacitance measurements, the open- and closed-circuit calibration of the LCR meter were performed while both probes were up in the air and while contacting each other, respectively.

Mechanical Testing: The sample used in the mechanical testing was cut into a dog-bone shape (as illustrated in Figure 3(a)-(c)) prior to the EGaIn deposition. The EGaIn traces were created using the air powered dispenser system by creating coalescing droplets and then sucking away the excess EGaIn using the vacuum function of the dispenser, forming a flat film. Glass masks were used during the sealing of the sample. After the formation of the electrodes, the samples were glued on each end to plates (on the top and the bottom) having two pin-holes. These plates were then inserted into the pins that were attached to the linear stages and further secured using screws. The axial loading was applied using a manual, lead-screw driven linear stage (Velmex UniSlide A15). The strain values were prescribed by the integrated precision position gage of lead screw drive and verified through image processing of the microscope images obtained using a stereo microscope (FireFly GT800). The resistance values for each deformation level and cycle were recorded 10 seconds after the sample is stretched, providing enough time for the resistance to settle to a final value.

Supporting Information

Supporting Information is available from the Wiley Online Library or from the author.

Acknowledgements

This work was supported by the Office of Naval Research Young Investigator Program (Program Officer Dr. Tom McKenna; Code 34).

Received: January 30, 2014
Revised: May 12, 2014
Published online:

[1] S. Cheng, Z. Wu, *Lab Chip* **2012**, *12*, 2782.
[2] S. Zhu, J.-H. So, R. Mays, S. Desai, W. R. Barnes, B. Pourdeyhimi, M. D. Dickey, *Adv. Funct. Mater.* **2013**, *23*, 2308.
[3] H. J. Kim, C. Son, B. Ziaie, *Appl. Phys Lett.* **2008**, *92*, 011904.
[4] R. D. P. Wong, J. D. Posner, V. J. Santos, *Sensor. Actuat. A-Phys.* **2012**, *179*, 62.
[5] Y. L. Park, B. R. Chen, R. J. Wood, *IEEE Sens. J.* **2012**, *12*, 2711.
[6] C. Majidi, R. Kramer, R. J. Wood, *Smart Mater. Struct.* **2011**, *20*, 105017.
[7] J. H. So, J. Thelen, A. Qusba, G. J. Hayes, G. Lazzi, M. D. Dickey, *Adv. Funct. Mater.* **2009**, *19*, 3632.
[8] S. Cheng, Z. Wu, P. Hallbjorner, K. Hjort, A. Rydberg, *IEEE T. Antenn. Propag.* **2009**, *57*, 3765.
[9] H. J. Koo, J.-H. So, M. D. Dickey, O. D. Velev, *Adv. Mater.* **2011**, *23*, 3559.
[10] J. H. So, H.-J. Koo, M. D. Dickey, O. D. Velev, *Adv. Funct. Mater.* **2012**, *22*, 625.
[11] S. Cheng, Z. Wu, *Adv. Funct. Mater.* **2011**, *21*, 2282.
[12] C. Majidi, Y.-L. Park, (co-1st author), R. Kramer, P. Bérard, R. J. Wood, *J. Micromech. Microeng.* **2010**, *20*, 125029.
[13] P. Roberts, D. D. Damian, W. Shan, T. Lu, C. Majidi, in *Proc. of the IEEE Conf. on Robotics and Automation* **2013**, 3529.
[14] D. M. Vogt, Y.-L. Park, R. J. Wood, *IEEE Sens. J.* **2013**, *13*, 4056.
[15] M. J. Regan, H. Tostmann, P. S. Pershan, O. M. Magnussen, E. DiMassi, B. M. Ocko, M. Deutsch, *Phys. Rev. B* **1997**, *55*, 10786.
[16] R. C. Chiechi, E. A. Weiss, M. D. Dickey, G. M. Whitesides, *Angew. Chem.* **2007**, *120*, 148.
[17] Q. Xu, N. Oudalov, Q. Guo, H. M. Jaeger, E. Brown, *Phys. Fluids* **2012**, *24*, 063101.
[18] M. D. Dickey, R. C. Chiechi, R. J. Larsen, E. A. Weiss, D. A. Weitz, G. M. Whitesides, *Adv. Funct. Mater.* **2008**, *18*, 1097.
[19] T. Liu, P. Sen, C. J. Kim, *J. Microelectromech. Syst.* **2012**, *21*, 443.
[20] S. H. Jeong, A. Hagman, K. Hjort, M. Jobs, J. Sundqvist, Z. Wu, *Lab Chip* **2012**, *12*, 4657.
[21] R. K. Kramer, C. Majidi, R. J. Wood, *Adv. Funct. Mater.* **2013**, *23*, 5292.
[22] A. Tabatabai, A. Fassler, C. Usiak, C. Majidi, *Langmuir* **2013**, *29*, 6194.
[23] A. Fassler, C. Majidi, *Lab on a Chip* **2013**, *13*, 4442.
[24] T. Lu, L. Finkenauer, J. Wissman, C. Majidi, *Adv. Funct. Mater.* **2014**, doi: 10.1002/adfm.201303732.
[25] J. W. Boley, E. L. White, G. T. C. Chiu, R. K. Kramer, *Adv. Funct. Mater.* **2014**, doi: 10.1002/adfm.201303220.
[26] C. Ladd, J. H. So, J. Muth, M. D. Dickey, *Adv. Mater.* **2013**, *25*, 5081.
[27] Y. Xia, G. M. Whitesides, *Angew. Chem. Int. Ed* **1998**, *37*, 550.
[28] R. Onler, B. A. Gozen, B. Ozdoganlar, in *Proc. of 8th Int. Conf. on Micro Manuf. ICOMM* **2013**, 30.
[29] S. Y. Chou, P. R. Krauss, P. J. Renstrom, *J. Vac. Sci. Technol. B* **1996**, *14*, 4129.
[30] D. Zrnic, D. Swatik, *J. Less-Common Metals* **1969**, *18*, 67.
[31] S. S. Gevorgian, P. L. J. Linner, E. L. Kollberg, *IEEE T. Microw, Theory.* **1996**, *44*, 896.
[32] A. Fassler, C. Majidi, *Smart Mater. Struct.* **2013**, *22*, 055023.